Araz Hashemi[1]
Department of Mathematics,
Wayne State University,
Detroit, MI 48202
e-mail: araz.hashemi@gmail.com

Yongcan Cao
Control Science Center of Excellence,
Air Force Research Laboratory,
Wright-Patterson AFB, OH 45433

David W. Casbeer
Control Science Center of Excellence,
Air Force Research Laboratory,
Wright-Patterson AFB, OH 45433

George Yin
Professor
Department of Mathematics,
Wayne State University,
Detroit, MI 48202

Unmanned Aerial Vehicle Circumnavigation Using Noisy Range-Based Measurements Without Global Positioning System Information

This work develops and analyzes a control algorithm for an unmanned aerial vehicle (UAV) to circumnavigate an unknown target at a fixed radius when the UAV is unable to determine its location and heading. Using a relationship between range-rate and bearing angle (from the target), we formulate a control algorithm that uses the range-rate as a proxy for the bearing angle and adjusts the heading of the UAV accordingly. We consider the addition of measurement errors and model the system with a stochastic differential equation to carry out the analysis. A recurrence result is proven, establishing that the UAV will reach a neighborhood of the desired orbit in finite time, and a mollified control is presented to eliminate a portion of the recurrent set about the origin. Simulation studies are presented to support the analysis and compare the performance against other algorithms for the circumnavigation task. [DOI: 10.1115/1.4027979]

1 Introduction

The global positioning system (GPS) has been the key tool enabling the ever-increasing use of unmanned aerial vehicles. Recently, the vulnerability of UAVs to GPS jamming and spoofing brings into question the reliability and safety of UAVs [1]. The aim of this paper is to investigate a control technique for circumnavigating a target in a GPS-denied environment and is motivated by the need for control authority given only range and possibly range-rate measurements [2]. Circumnavigation is the act of orbiting an object of interest at a fixed distance and is useful for tracking and surveilling targets [3,4].

The problem of circumnavigation has been investigated considering both relative measurements between the target and UAV [4] as well as with bearing only measurements [5]. Circumnavigation using range (and possibly range-rate) measurements has been analyzed in Ref. [6] by designing a control that satisfies a persistent excitation condition, and the underlying policy relies on the UAV knowing its own position in some reference frame. Another recent publication utilized a sliding-mode controller to achieve the desired orbit about the target of interest, however the stability results are not global [7].

The groundwork for this paper comes from Refs. [8] and [9], where in Ref. [8] the authors proved global stability to the desired orbit using range and range-rate measurements without the need for an underlying reference frame. Preliminary work has been investigated to determine the feasibility of such a control policy by estimating the range-rate from range observations [10]. The effects of noise on the stability of a modified control were presented in Ref. [9], where using recurrence analysis it was shown that the UAV would reach a neighborhood of the desired orbit in finite time.

In this paper, we clarify and elaborate on the results in Ref. [9]. First, because of two unstable equilibrium inside the desired orbit, the recurrence analysis in Ref. [9] yields two disjoint sets in which the UAV could return infinitely often. The outer recurrent subset is a ring containing the orbit of interest, while the other is a ball around the origin. In this paper, a mollified control is presented that eliminates the recurrent set about the origin, while maintaining the continuity properties requisite for applying existing stochastic stability results. Furthermore, additional simulations have been added, which compare the proposed "switching" control with a Dubins-type control [11] for the same task to evaluate performance.

The organization of the paper is as follows: In Sec. 2, the problem of circumnavigation using range and range-rate measurements is formally laid out. Section 3 presents the control policy and is followed by stochastic stability analysis in Sec. 4. Due to the inner unstable equilibrium, a mollified controller is presented in Sec. 5. Simulations and comparison with competing algorithms are carried out in Sec. 6, which is followed by concluding remarks.

2 Problem Formulation

Let us begin with the deterministic model for the circumnavigation problem. Assuming the UAV travels at a constant velocity V, the dynamics are given by

$$\begin{aligned} \dot{x} &= V\cos(\psi) \\ \dot{y} &= V\sin(\psi) \\ \dot{\psi} &= u \end{aligned} \tag{1}$$

where $[x,y]$ is the 2D location of the UAV, ψ is the heading angle of the UAV, and u is the heading rate to be controlled. The goal for the circumnavigation task is to design a control algorithm for u such that the UAV orbits an unknown (fixed) target at a desired radius r_d. Without GPS, we assume that only the range r from the target is available, as well as the range-rate $\dot{r}$.

To ease notation in the analysis, we take the target T as the origin of our coordinate frame. For the analysis, we will make use of the reference angle ϕ to the UAV (from the target T at (0, 0)), as well as the local heading angle ψ of the UAV and the bearing angle θ from the reference vector to the heading vector. These

[1]Corresponding author.

Contributed by the Dynamic Systems Division of ASME for publication in the Journal of Dynamic Systems, Measurement, and Control. Manuscript received January 29, 2014; final manuscript received June 24, 2014; published online October 21, 2014. Assoc. Editor: Dejan Milutinovic.

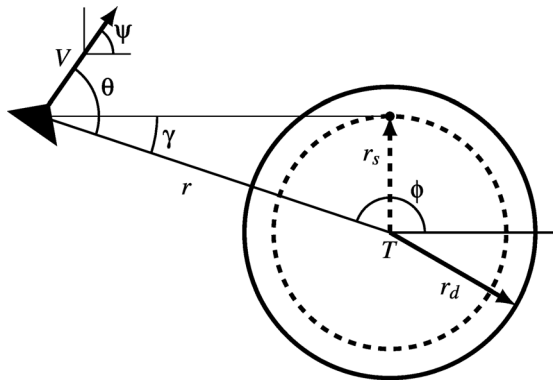

Fig. 1 We design a control which aims at the tangent of the orbit of radius r_s, but will "stabilize" at the orbit of radius r_d. Here, $\gamma = \sin^{-1}(r_s/r)$.

angles can be seen in Fig. 1. We note that the angles can be related by the equation

$$\theta = \pi - \phi + \psi \tag{2}$$

Using Eq. (2), one can obtain $\dot{r} = -V\cos\theta$. This gives a correspondence between the bearing angle θ and the range-rate $\dot{r}$. We exploit this relationship to use $\dot{r}$ as a proxy for θ in the design of our control. Similarly, it can be seen that $\dot{\theta} = V\sin\theta/r + u$. Thus we change the variables from $\{(x, y, \phi)\}$ in Eq. (1) to $\{(r, \theta)\}$ given by

$$\begin{aligned} \dot{r} &= -V\cos\theta \\ \dot{\theta} &= \frac{V\sin\theta}{r} + u \end{aligned} \tag{3}$$

which reduces the complexity of the system to only two variables, one of which we can directly observe (r) and the other we can determine from $\dot{r}$. When the circumnavigation task is accomplished $r = r_d$ and $\theta = \pi/2$ (for clockwise orbit) or $\theta = 3\pi/2$ (for counterclockwise orbit). In the development we default to a clockwise orbit ($\theta = \pi/2$), but both will be considered. Thus, we desire a control $u(r, \dot{r}) = u(r, -V\cos\theta)$ such that the dynamics drive (r,θ) to $(r_d, (\pi/2))$.

3 The Control Algorithm

We design the control algorithm in two cases: (1) $r \geq r_s$; and (2) $r < r_s$, where $r_s = \sqrt{r_d^2 - (1/k^2)}$ for some $k > 0$ is a "singular" orbit which the UAV shall aim for in order to stabilize at the desired orbit of r_d. We develop the algorithm in the two cases as follows.

3.1 Outer Control. Here, we consider $r \geq r_s$, i.e., the UAV is outside of the dashed circle in Fig. 1. The idea for the control algorithm is to drive the UAV toward the tangent point on the dashed circle from the current UAV location. We distinguish between the singular orbit at r_s (dashed line) being aimed for and the desired orbit at r_d (solid line) because we shall see that the UAV cannot stabilize at the orbit being aimed for. However, it will be seen that the orbit aimed for at r_s can be chosen so that given a gain size k and a desired orbit at r_d, aiming for an orbit at $r_s = \sqrt{r_d^2 - (1/k^2)}$ will result in the UAV stabilizing at an orbit of r_d. Thus, we currently focus on the task of aiming for an orbit at r_s.

Figure 1 depicts the task of aiming the UAV toward the singular orbit at r_s. Denoting $\gamma = \sin^{-1}(r_s/r)$, we wish to adjust ψ so that $\theta = \gamma$. But without the ability to measure ψ, it is not possible to make a direct adjustment. Instead we only have $\dot{r}$ as a proxy for $-V\cos\theta$. Given the preference that the UAV orbit clockwise (so that $\theta, \gamma \in [0, \pi]$), $\cos(\cdot)$ is decreasing on $[0, \pi]$. It is then seen that $\cos\theta - \cos\gamma \leq 0$ for $\theta \geq \gamma$, and $\cos\theta - \cos\gamma \geq 0$ for $\theta \leq \gamma$. Thus

$$-k\left[\dot{r} + V\cos\sin^{-1}\frac{r_s}{r}\right] = kV(\cos\theta - \cos\gamma)\begin{cases} < 0, & \theta > \gamma \\ > 0, & \theta < \gamma \end{cases} \tag{4}$$

This motivates us to define a control for outside r_s by

$$\begin{aligned} u_o(r, \dot{r}) &= -\lambda k\left[\dot{r} + V\cos\sin^{-1}\left(\frac{r_s}{r}\right)\right]\mathbb{I}_{\{r \geq r_s\}} \\ &\text{or equivalently} \\ u_o(r, \theta) &= \lambda k\left(V\cos\theta - V\frac{\sqrt{r^2 - r_s^2}}{r}\right)\mathbb{I}_{\{r \geq r_s\}} \end{aligned} \tag{5}$$

where $\lambda \in \{+1, -1\}$ is a flag variable and k is a positive constant. The main idea behind the proposed controller (5) is to adjust the heading of the UAV such that the UAV moves toward one of the two tangent points on the circle centered at T with radius r_s (see Fig. 1 for an illustrative example). The flag variable λ is used solely to determine whether the UAV exhibits a clockwise or counterclockwise motion. For the clarity of presentation, λ is set to $+1$ when technical analysis is conducted for Eq. (5), but similar analysis can be applied for the case $\lambda = -1$ to obtain similar results. One noticeable feature for Eq. (5) is its boundedness by $2kV$.

As stated previously, the UAV does not stabilize at an orbit of radius r_s. Assume a stable circular orbit exists with its radius r_a. If a trajectory given by Eq. (3) is stable at r_a, then we must have $\dot{r} = 0$. Then using $u_o(r, \dot{r})$ as in Eq. (5), the nominal angular velocity $|V/r_a| = |\dot{\psi}| = |u(r_a, 0)|$, giving that $(V/r_a) = kV\cos\sin^{-1}(r_s/r_a) = kV(\sqrt{r_a^2 - r_s^2}/r_a)$ and so $r_a^2 = (1/k^2) + r_s^2$. Because $r_s = \sqrt{r_d^2 - (1/k^2)}$ as seen at the beginning of the section, r_a is exactly the same as r_d, meaning that the UAV stabilizes at an orbit of the desired radius.

3.2 Inner Control. For $r < r_s, \cos\sin^{-1}(r_s/r)$ is not well defined due and thus neither is the control given in Eq. (5). In this case, another control is needed for inside the dashed circle in Figs. 1 and 2. In Ref. [8], zero control input is applied in order to drive the UAV outside the red dashed circle. A disadvantage of such a control strategy (i.e., zero control for inside the dashed

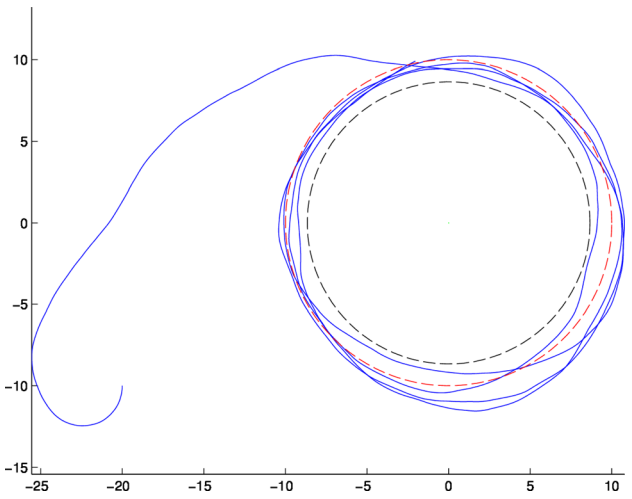

Fig. 2 A sample trajectory under u_o with small gain: $k = 0.2$, $r_d = 10$, $r_s = 8.67$, $V = 1$, and additive white measurement noise $\sigma = 0.5$

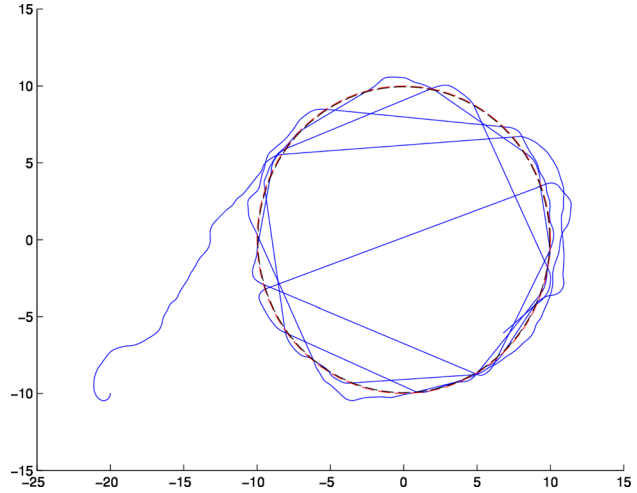

Fig. 3 A sample trajectory under u_o, with large gain: $k = 1$ corresponding to $r_s = 9.95$. When measurement error nudges the UAV past the r_s threshold, it cuts across the circle.

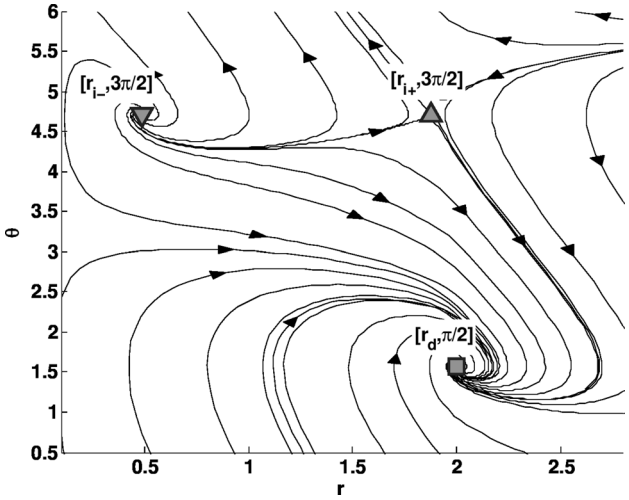

Fig. 4 Phase portrait of Eq. (3) using $u = u_o + u_i$ with $k = 2.118$, $V = 1$, $r_s = 1.9345$, and $r_d = 2$

circle) is that the UAV has to move outside the dashed circle before control takes affect. As shown in Fig. 3, the performance is degraded if the UAV moves inside the inner dashed circle quite often. This is particularly true when range and/or range-rate measurements are noisy and r_d is close to r_s for large k. Given this insight into the behavior of the controller, we seek to develop a controller for when the UAV is inside the circle of radius r_s.

To obtain this controller, we first look at the outer controller to gain insight into what modifications will yield an acceptable controller for inside the red dashed circle. Note that the two terms in $u_o(r,\theta) = kV\cos\theta - kV(\sqrt{r^2 - r_s^2}/r)$ work separately to adjust the bearing angle and radius. If $\theta < (\pi/2)$ (the bearing is too acute), then $kV\cos\theta$ is positive and drives the UAV counterclockwise, and does the reverse if $\theta > (\pi/2)$. However, if $r > r_s$, then $(-kV/r)\sqrt{r^2 - r_s^2}$ adjusts the heading in such a way that the UAV rotates toward heading the target. This suggests the following inner control as:

$$u_i(r,\dot{r}) = -\lambda k\left[\dot{r} - V\cos\sin^{-1}\left(\frac{r}{r_s}\right)\right]\mathbb{I}_{\{r<r_s\}}$$

or equivalently

$$u_i(r,\theta) = \lambda k\left(V\cos\theta + \frac{V}{r_s}\sqrt{r_s^2 - r^2}\right)\mathbb{I}_{\{r<r_s\}} \tag{6}$$

where λ is the same flag variable used in Eq. (5) and k is a positive constant. Notice that the first component in Eq. (6) is the same as the first component in u_o, but the second component is negated with the nominator and denominator flipped. In the subsequent analysis, λ is set to be $+1$ for the clarity of presentation. All results hold similarly for $\lambda = -1$.

Again, an "equilibrium" orbit of radius $r_i < r_s$ is possible. If such an orbit exists, it must satisfy $|V/r_i| = |u_i(r_i,0)|$ (using the definition in terms of $u_i(r,\dot{r})$). By computation, one can obtain

$$r_i^2 = \frac{1}{2}\left[r_s^2 - \sqrt{r_s^4 - \frac{4}{k^2}r_s^2}\right]$$
$$= \frac{1}{2}\left(r_d^2 - \frac{1}{k^2}\right) \pm \frac{1}{2}\sqrt{\left(r_d^2 - \frac{1}{k^2}\right)\left(r_d^2 - \frac{5}{k^2}\right)} \tag{7}$$

which has no solution for $k \in (1/r_d, \sqrt{5}/r_d)$, but otherwise has two solutions $r_{i-} = [(1/2)(r_d^2 - (1/k^2)) - (1/2)\sqrt{(r_d^2 - (1/k^2))(r_d^2 - (5/k^2))}]^{\frac{1}{2}}$ and $r_{i+} = [(1/2)(r_d^2 - (1/k^2)) + (1/2)\sqrt{(r_d^2 - (1/k^2))(r_d^2 - (5/k^2))}]^{\frac{1}{2}}$. In particular, $r_{i-} \to 0$ and $r_{i+} \to r_d$ as $k \to \infty$. We will refer back to these in the recurrence analysis.

Remark 3.1. We note that the UAV can only stabilize at one inner equilibrium radius if the initial point and heading is exactly along the orbit with radius r_{i-} (respectively, r_{i+}) in a counterclockwise orientation, corresponding to $(r(0),\theta(0)) = (r_{i-}, 3\pi/2)$ [respectively, $(r(0),\theta(0)) = (r_{i+}, 3\pi/2)$], thus forcing the "$\theta$" (or $\dot{r}$) component of the control $kV\cos\theta$ in Eq. (6) to be 0. However, any perturbation of the inputs for the control, forcing the UAV even negligibly off-course, will cause the θ component to drive the UAV's bearing angle toward $\pi/2$ because $(r_{i-}, 3\pi/2)$ [respectively, $(r_{i+}, 3\pi/2)$] is an unstable equilibrium. This assertion is further confirmed in Fig. 4, from which we can see that both $(r_{i-}, 3\pi/2)$ and $(r_{i+}, 3\pi/2)$ are unstable equilibriums. Eventually, the UAV will be driven outside the orbit with radius r_s. In the presence of measurement errors, the UAV is driven outside the orbit with radius r_s almost immediately as evidenced by Fig. 6. Other simulations demonstrate that even if $(r(0),\theta(0)) = (r_{i-}, 3\pi/2)$ [respectively, $(r(0),\theta(0)) = (r_{i+}, 3\pi/2)$] and no measurement errors exist, accumulated numerical errors will eventually drive the UAV slightly off the orbit of radius r_i after which it immediately moves outside the orbit with radius r_s. Hence the inner equilibrium orbits are of little practical concern for the implementation of the control algorithm.

To summarize, the proposed switching control algorithm is given by $u = u_o + u_i$; that is

$$u(r,\dot{r}) = -\lambda k\dot{r} - \lambda kV\cos\sin^{-1}\left(\frac{r_s}{r}\right)\mathbb{I}_{\{r>r_s\}}$$
$$+ \lambda kV\cos\sin^{-1}\left(\frac{r}{r_s}\right)\mathbb{I}_{\{r<r_s\}} \tag{8}$$

or equivalently

$$u(r,\theta) = \lambda kV\cos\theta - \frac{\lambda kV}{r}\sqrt{r^2 - r_s^2}\,\mathbb{I}_{r>r_s} + \frac{\lambda kV}{r_s}\sqrt{r_s^2 - r^2}\,\mathbb{I}_{r<r_s}$$

As an example, Figs. 5 and 6 depict the improved performance of the UAV under the proposed control algorithm (8) with $k = 1$ using noisy measurements. The other parameters are as in Fig. 3; i.e., $r_d = 10$, $r_s = 9.95$, and the magnitude of the measurement noise is $\sigma = 0.5$. Notice that the UAV will eventually stay close to the desired orbit as opposed to the behavior seen in Fig. 3 when zero control is applied for the case $r(t) < r_s$. Thus we see

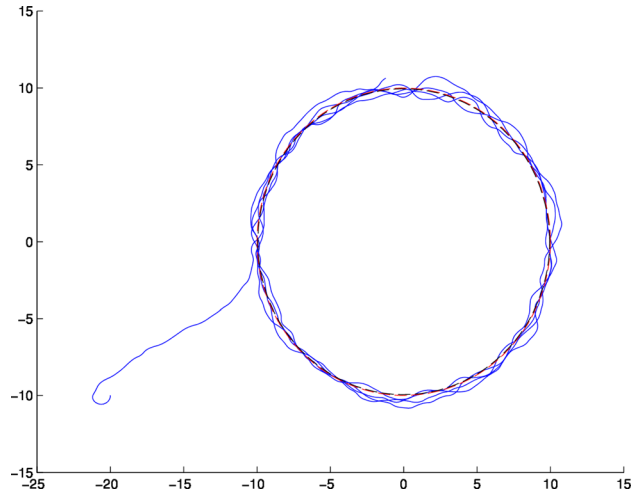

Fig. 5 A sample trajectory under u using noisy measurements with initial point outside the desired orbit

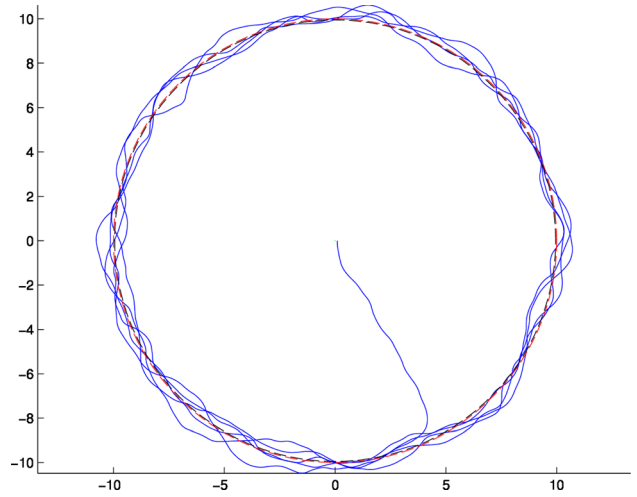

Fig. 6 Sample trajectory under u using noisy measurements with initial point inside the desired orbit

substantial improvement from the "outer-only" control u_o depicted in Fig. 3.

4 Measurement Error Analysis

4.1 SDE Formulation. Here, we formally introduce additive measurement noises in the controller. For example, range r can be measured accurately, but range-rate measurement is noisy $\tilde{\dot{r}} = \dot{r} + \nu$ where $\nu \sim \mathcal{N}(0, \sigma)$. This model has practicality, as the range measurements are tremendously accurate compared to range-rate measurements regardless of what method we use for the estimation. Then the noisy control input becomes $\tilde{u}(r, \theta, \nu) \triangleq u(r, \dot{r} + \nu) \triangleq u(r, \theta) - k\nu$. With the noisy control input, the noisy system dynamics are modeled by the following stochastic differential equation (SDE):

$$d\begin{bmatrix} r \\ \theta \end{bmatrix} = \begin{bmatrix} -V\cos\theta \\ \dfrac{V\sin\theta}{r} + u(r,\theta) \end{bmatrix} dt + \begin{bmatrix} 0 \\ -k\sigma \end{bmatrix} d\xi \tag{9}$$

where ξ is a standard Brownian motion.

The error introduced into θ by the diffusion term then integrates into the dynamics in r, giving stochastic dynamics for both state variables. We note that with the Lyapunov approach which follows one may also consider nonzero diffusion coefficient σ_r for r in Eq. (9) and obtain the same results, since the proposed Lyapunov function $\mathcal{V}(r, \theta)$ will have $\partial/(\partial r)^2\mathcal{V} = 0$. This model would be more appropriate in the case that there is noise in r independent of the noise in $\dot{r}$. However, in line with the motivation that estimates of $\dot{r}$ have much higher variance than measurements of r, we shall remain with zero diffusion coefficient for r in Eq. (9).

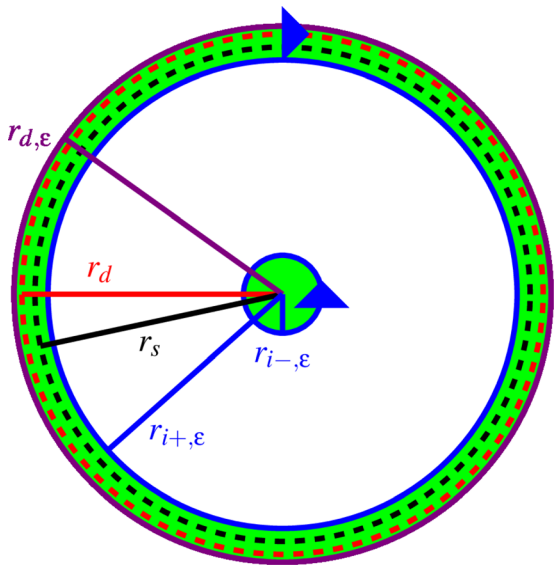

Fig. 7 The recurrent set $U_{k,\varepsilon}$

One can verify that the control defined by Eq. (8) has linear growth and is Lipschitz continuous (even at $r = r_s$), and the other coefficients also satisfy this property on domains bounded away from $r = 0$ (see the Appendix for a short proof). Hence, Eq. (9) describes an Itô diffusion, and thus a unique Markov solution exists for the trajectory as in Ref. [12, Definition 7.1.1, Theorem 5.2.1]. The associated generator $\mathcal{L}$ of the diffusion is given by

$$\mathcal{L}\mathcal{V}(r,\theta) = [-V\cos\theta]\frac{\partial}{\partial r}\mathcal{V}(r,\theta) + \left[\frac{V\sin\theta}{r} + u(r,\theta)\right]\frac{\partial}{\partial\theta}\mathcal{V}(r,\theta) + \frac{k^2\sigma_{rr}^2}{2}\frac{\partial^2}{\partial\theta^2}\mathcal{V}(r,\theta) \tag{10}$$

4.2 A Recurrence Result. Let $Z(t)$ be an ℓ-dimensional diffusion process. It is said to be regular if it does not blow up in finite time w.p.1. Suppose that $Z(t)$ is an ℓ-dimensional diffusion process that is regular, that D is an open set with compact closure, that $Z(0) = z \in D^c$ the complement of D, and that $\sigma_D^z = \inf\{t : Z^z(t) \in D\}$, where $Z^z(t)$ signifies the initial data z-dependence of the diffusion. The process $Z^z(\cdot)$ is recurrent with respect to D if $P(\sigma_D^z < \infty) = 1$ for any $z \in D^c$; otherwise, the process is transient w.r.t. (with respect to) D. A recurrent process with finite mean recurrence time w.r.t. D is said to be positive recurrent w.r.t. D; otherwise, the process is null recurrent w.r.t. D.

Coming back to our problem, we shall show that the trajectory of the UAV under control policy (8) with dynamics given by Eq. (9) is recurrent with respect to a neighborhood of either $r = r_d$ or $r = 0$, as depicted in Fig. 7. Again, we take the convention of a clockwise orbit (so $\lambda = 1$, though $\lambda = -1$ works similarly). The recurrence is in the sense that if the initial point of the UAV is outside of the recurrent set, the UAV will enter the recurrent set in finite time almost surely. We note that stronger notions of convergence and stability (such as almost-sure, exponential, and p-stability as in Ref. [13]) are not possible since in our model the noise is "persistent" and does not decay at the equilibrium point.

Hence, recurrence is the appropriate notion of convergence for the system (9).

We prove our result using a Lyapunov function approach. Consider the candidate function

$$\mathcal{V}(r,\theta) = \frac{k}{V}|r - r_s| + \frac{\theta}{V}\text{sgn}(r - r_s) + \frac{2\pi}{V} \tag{11}$$

which is everywhere positive in the domain $r \in (0, r_s) \cup (r_s, \infty)$ and $\theta \in [0, 2\pi)$. Note that $\mathcal{V}$ by Eq. (11) is not differentiable along $r = r_s$. However, this will become part of the recurrent set $U_{k,\varepsilon}$ and it is only on the complement set $U^c_{k,\varepsilon}$, where the Lyapunov function must be smooth. On such a domain, we have that

$$\mathcal{LV} = \frac{\sin\theta}{r}\text{sgn}(r - r_s) - \frac{k}{r}\sqrt{r^2 - r_s^2}\mathbb{I}_{\{r>r_s\}} - \frac{k}{r_s}\sqrt{r_s^2 - r^2}\mathbb{I}_{\{r<r_s\}} \tag{12}$$

We note that in the $\lambda = -1$ case, one should take the Lyapunov function $\mathcal{V}(r,\theta) = (k/V)|r - r_s| + (\theta/V)\text{sgn}(r_s - r)$ to get the same expression as Eq. (12) except with the negation of the first term. This will result in similar analysis as below, except that the "worst-case" scenario for the most positive $\mathcal{LV}$ could be occurs when $\theta = (3\pi/2)$.

THEOREM 4.1. *For ε sufficiently small (given by Remark 4.3) and k sufficiently large ($k \geq 1/r_d$), there exist*

$$\begin{array}{llll} r_{i-,\varepsilon} \searrow r_{i-} & r_{i+,\varepsilon} \nearrow r_{i+} & r_{d,\varepsilon} \searrow r_d & \text{as } \varepsilon \downarrow 0 \\ \text{where} & & & \\ r_{i-} \searrow 0 & r_{i+} \nearrow r_s & r_s \nearrow r_d & \text{as } k \uparrow \end{array} \tag{13}$$

such that $\mathcal{LV} \leq -\varepsilon$ on $U^c_{k,\varepsilon}$, where

$$U_{k,\varepsilon} \triangleq \{(0, r_{i-,\varepsilon}) \times (\pi, 2\pi)\} \cup \{(r_{i+,\varepsilon}, r_{d,\varepsilon}) \times (0, \pi)\} \tag{14}$$

Given that $\mathcal{V}$ by Eq. (11) is positive on its domain, using the above with Ref. [13, Theorem 3.9] we obtain the following result.

COROLLARY 4.2 (Recurrence Time Bound). *Reference [13] For ε sufficiently small and k sufficiently large, the trajectory of the UAV derived from Eq. (9) under control policy Eq. (8) is recurrent w.r.t. $U_{k,\varepsilon}$ as defined in Eq. (14). Given an initial point (r_0, θ_0), the expected recurrence time τ_ε until the UAV reaches $U_{k,\varepsilon}$ is bounded by*

$$\mathbb{E}^{(r_0,\theta_0)}\tau_\varepsilon \leq \frac{\mathcal{V}(r_0,\theta_0)}{\varepsilon} = \frac{k|r_0 - r_s| + \theta_0 + 2\pi}{V\varepsilon} \tag{15}$$

Proof of Theorem 4.1. Note that the second and third terms of Eq. (12) are always nonpositive. If $r > r_s$ and $\theta \in (\pi, 2\pi)$ then $\mathcal{LV} < 0$. Similarly if $r < r_s$ and $\theta \in (0, \pi)$, then $\mathcal{LV} < 0$. We also note that $\mathcal{LV} \leq 0$ for $r \geq r_d$, regardless of θ. In particular, considering the worst-case scenario $\sin\theta = 1$ we can solve for $r > r_s$ such that $\mathcal{LV}(r) = (1/r)\left[1 - k\sqrt{r^2 - r_s^2}\right] \leq -\varepsilon$. This has a solution if $\varepsilon \leq k$ (where k can be taken in $[(1/r_d), \infty)$) and leads us to define

$$r_{d,\varepsilon} \triangleq \frac{\varepsilon + \sqrt{k^2 r_d^2[k^2 - \varepsilon^2] + \varepsilon^2}}{k^2 - \varepsilon^2} \tag{16}$$

Then $\mathcal{LV}(r,\theta) \leq -\varepsilon$ for $r \geq r_{d,\varepsilon}$ regardless of θ. As $\varepsilon \downarrow 0$ or as $k \uparrow \infty$, we have $r_{d,\varepsilon} \downarrow r_d$. Thus we can force $r_{d,\varepsilon}$ arbitrarily close to r_d.

If $r < r_s$, then $\mathcal{LV} = (-\sin\theta/r) - (k/r_s)\sqrt{r_s^2 - r^2}$. Again considering the worst-case scenario $\sin\theta = -1$, we inspect the function $g(r) = (1/r) - (k/r_s)\sqrt{r_s^2 - r^2}$ and solve for r_i such that $g(r_i) = 0$. This reduces to Eq. (7), which has no solutions in $(0, r_s)$ for $k \in (1/r_d, \sqrt{5}/r_d)$, but otherwise has two solutions $r_{i-} \to 0$ and $r_{i+} \to r_d$ as $k \to \infty$. If $r_{i-} \leq r \leq r_{i+}$, then $\mathcal{LV} \leq 0$. If $k < \sqrt{5}/r_d$, then $\mathcal{LV}$ is always positive in a neighborhood of $\theta = 3\pi/2$ for all $0 < r \leq r_s$.

Repeating the process to solve where $g(r) = -\varepsilon$, we obtain the quartic equation $r^4 + (r_s^2/k^2)(\varepsilon^2 - k^2)r^2 - 2\varepsilon(r_s^2/k^2)r + (r_s^2/k^2) = 0$ which has two solutions $r_{i-,\varepsilon}$ and $r_{i+,\varepsilon}$ in (r_{i-}, r_{i+}) for sufficiently small ε. Between $r_{i-,\varepsilon}$ and $r_{i+,\varepsilon}$ we have that $g(r) \leq -\varepsilon$, with $r_{i-,\varepsilon} \downarrow r_{i-}$ and $r_{i+,\varepsilon} \uparrow r_{i+}$ as $\varepsilon \downarrow 0$. Then using $r_{i-} \searrow 0$, $r_{i+} \nearrow r_s$, and $r_s \nearrow r_d$ as $k \uparrow$, the corollary stands. □

Remark 4.3 (ε Upper Bound). One sees that the upper bound on the recurrence time τ_ε given in Corollary 4.2 is inversely proportional to ε (corresponding to the size of the recurrent set $U_{k,\varepsilon}$). This is intuitive, as allowing for a larger neighborhood of the desired orbit decreases the bound for the time τ_ε it takes to reach said neighborhood. One may wonder how large we may take ε to be while still being able to solve for a recurrent set $U_{k,\varepsilon}$, off of which $\mathcal{LV} \leq -\varepsilon$. To find the maximum value of ε which allows for the result, one may analyze the function $g(r) = (1/r) - (k/s)\sqrt{s^2 - r^2}$, where $s = \sqrt{r_d^2 - k^{-2}}$ varies with k but is bounded between 0 and r_d. Heuristically, one sees that the minimum value of $g(r)$ is $-O(k)$, and thus the maximum possible value of ε is $O(k)$. The explicit bound can be found by finding the unique solution of $g'(r_*) = 0$ in (r_{i-}, r_{i+}) whose evaluation in $g(r_*)$ gives the lower bound needed for the analysis inside $r < r_s$. Thus taking $\varepsilon < \min\{g(r_*), r_d^{-1}\}$ will yield a valid result.

Remark 4.4 (k"Practical" Upper Bound). For a fixed value of k, one may let $\varepsilon \searrow 0$ and obtain a "minimal" recurrent set $U_k = \{(0, r_{i-}) \times (\pi, 3\pi/2)\} \cup \{(r_{i+}, r_d) \times (0, \pi)\}$. While analytically one may take k arbitrarily large to force $r_{i-} \searrow 0$ and $r_{i+} \nearrow r_s \nearrow r_d$ and tighten the minimal recurrent set, practically one encounters problems if the gain is too large. In practice, one applies the control at discrete time steps instead of continuously, and this results in non-smooth control. If the maximum control effort $2kV$ is larger than π, then (in addition to clearly violating practical turning constraints) it is possible for the UAV to spin out, resulting in significant deviations from the desired orbit. We shall observe this in the simulation study, e.g., Fig. 10.

5 Mollified Switching Controller

As mentioned in Remark 3.1, the inner equilibrium orbits or radii r_{i+} and r_{i-} are not stable and simulations have shown even numerical errors will quickly drive the UAV outside the singular orbit r_s. However, they do present some problems in the theoretical analysis. For one, the deterministic system (3) does not have a unique equilibrium. Furthermore, the recurrent set $U_{k,\varepsilon}$ as depicted in Fig. 7 has a possible inner component which does not contain the desired orbit. Again, while simulations show that this set is not stable it is desirable to ensure analytically that the UAV will in fact recur to a neighborhood of the desired orbit.

The simplest way to remove the inner equilibrium orbits (and inner component of the recurrent set) is to switch to zero control when $r \leq r_{i+}$ so that the inner limit cycles are no longer possible. However, this is not smooth at $r = r_{i+}$ when $\cos\theta \neq 0$. We amend this by mollifying the control to 0 uniformly in a small neighborhood of $r = r_{i+}$ as follows. Let $\chi_\delta(x)$ be a smooth cut-off function such that

$$\chi_\delta(r) \triangleq \begin{cases} 1 & \text{if } r > r_{i+} + \delta \\ 0 & \text{if } r \leq r_{i+} \\ \text{smooth} & \text{otherwise} \end{cases} \tag{17}$$

define

$$u_\delta(r,\theta) \triangleq u(r,\theta)\chi_\delta(r) \tag{18}$$

with the understanding that if $(1/r_a) \leq k < (\sqrt{5}/r_a)$, then $r_{i+} \triangleq 0$. Then u_δ is everywhere smooth, u_δ takes the same value as u for

$r \notin (r_{i+}, r_{i+} + \delta)$, and u_δ has the same sign as u on all of $\mathbb{R}^n$. For the remainder of this section, assume $\lambda = +1$ (corresponding to a clockwise orbit) for convenience of notation.

We mention that with the mollified control u_δ, we have shown that the deterministic system (from Eq. (9) with $\sigma = 0$) has unique limit $(r_d, \pi/2)$ (or $(r_d, 3\pi/2)$ for $\lambda = -1$). Since u_δ takes the same sign as u, we can show that under control u_δ, the deterministic trajectory $(r(t), \theta(t))$ as $t \to \infty$ using methods similar to Ref. [8]. For brevity, we omit the presentation of the deterministic limit in favor of focusing on the stochastic result.

We now examine the properties of the stochastic system given in Eq. (9) under the mollified control u_δ. Since u is globally Lipschitz with linear growth (as shown in the Appendix) and u_δ is a smooth mollification of u, we have u_δ also satisfies the Lipschitz and linear growth condition. Thus the diffusion (9) has a unique Markovian solution with generator

$$\mathcal{L}\mathcal{V}(r,\theta) = [-V\cos\theta]\frac{\partial}{\partial r}\mathcal{V}(r,\theta) + \left[\frac{V\sin\theta}{r} + u_\delta(r,\theta)\right]\frac{\partial}{\partial\theta}\mathcal{V}(r,\theta) + \frac{k^2\sigma_{rr}^2}{2}\frac{\partial^2}{\partial\theta^2}\mathcal{V}(r,\theta) \tag{19}$$

Assume for the remainder of this section that $\delta < \min\{k, r_d - r_{i+}\}$. Take $r_{d,\delta}$ as in Eq. (16). Then we have the following result.

THEOREM 5.1. *Let $U_\delta = \{(r,\theta) : r < r_{d,\delta}\}$. Then the trajectory $r(t), \theta(t)$ of Eq. (9) under control policy u_δ is recurrent to U_δ. Given initial point (r_0, θ_0) with $r_0 > r_d$, the expectation of the stopping time τ_δ until the UAV reaches U_δ is bounded by*

$$\mathbb{E}\tau_\delta \le \frac{k(r_0 - r_d) + \theta_0}{V\delta} \tag{20}$$

Proof. Consider the Lyapunov function $\mathcal{V}(r,\theta) \triangleq ((k(r - r_d) + \theta)/V)$. Conducting the analysis on the set $U_\delta^c = \{(r,\theta) : r \ge r_{d,\delta}\}$, we have that $\mathcal{L}\mathcal{V} = (1/r)\left(\sin\theta - k\sqrt{r^2 - r_s^2}\right)$. At most, $\sin\theta = 1$ for which $(1/r)\left(1 - k\sqrt{r^2 - r_s^2}\right) \le -\delta$ for $r \ge r_{d,\delta}$. Thus $\mathcal{L}\mathcal{V} \le -\delta$ on U_δ^c, and by Ref. [13, Theorem 3.9] the theorem follows. □

For $r \le r_{i+}$, the UAV applies zero control, and thus must fly straight until it exits $\{(r,\theta) : r < r_{i+}\}$ in time less than $2r_{i+}/V$. Hence, we obtain the following global recurrence result to a neighborhood of the desired orbit of radius r_d.

COROLLARY 5.2. *For any initial point (r_0, θ_0) the UAV under policy u_δ in Eq. (9) is recurrent to the set $\tilde{U}_{k,\delta} \triangleq \{(r,\theta) : r_{i+} \le r \le r_{d,\delta}\}$. The expectation of the stopping time $\tilde{\tau}_\delta$ until the UAV reaches $\tilde{U}_\delta$ is bounded by*

$$\mathbb{E}\tilde{\tau}_\delta \le \max\left\{\frac{k(r_0 - r_d) + \theta_0}{V\delta}, \frac{2r_{i+}}{V}\right\} \tag{21}$$

6 Simulation Study

6.1 Measurement Error, Windless. Here, we simulate the performance of the control algorithm (8) with additive measurement errors in the absence of wind, as in Eq. (9). The desired orbit is of radius $r_d = 10$. We take the velocity of the UAV $V = 1$ and the standard deviation of the measurement error $\sigma = 0.5$. We run the simulation for 350 s, updating the control every 0.5 s. Figure 8 shows the trajectory of UAV with gain size $k = 0.1 = r_d^{-1}$ corresponding to $r_s = 0$, while Fig. 9 shows the trajectory with gain size $k = 1.0$ corresponding to $r_s = 9.95$. We observe that the smaller gain size gives a smoother trajectory but larger deviations from the desired radius. The larger gain size adheres to the desired orbit more closely, but at the expense of a larger control effort.

We then run the simulation 20 times, increasing the gain k on each iteration from the minimum value $k = 0.1$ by increments of 0.15, and collect statistics its performance. Figures 10 and 11 show the average (over the 350 s length of each simulation) of $(r - r_d)^2$ and $\dot{r}^2$, respectively, as the gain k increases. This supports the observation from the trajectories that higher gain choices

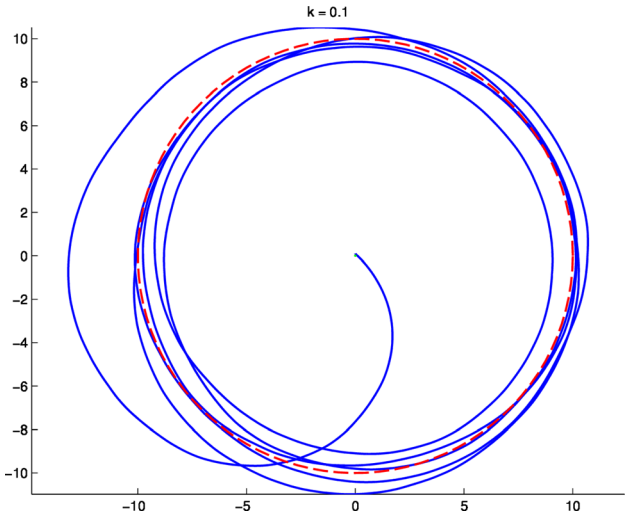

Fig. 8 Trajectory with measurement error, $k = 0.1$

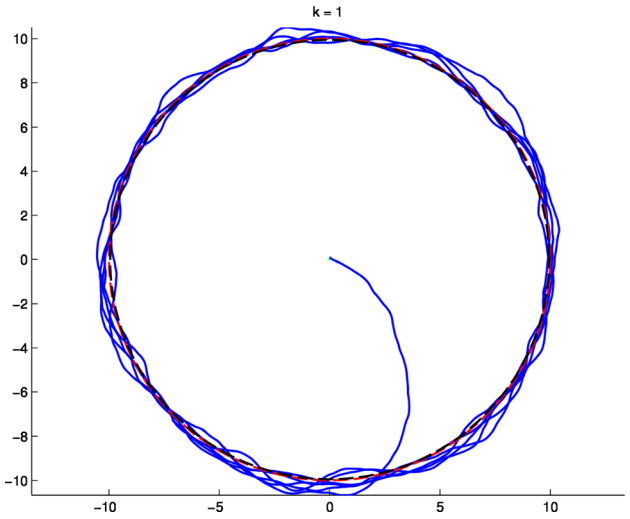

Fig. 9 Trajectory with measurement error, $k = 1$

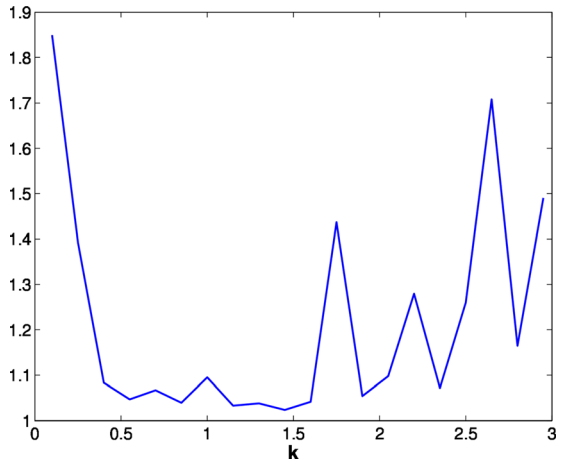

Fig. 10 Average value of error $(r - r_d)^2$ for different values of k

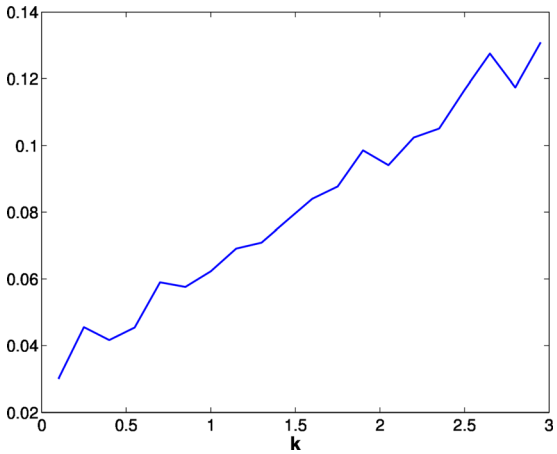

Fig. 11 Average value of $\dot{r}^2$ for different values of k

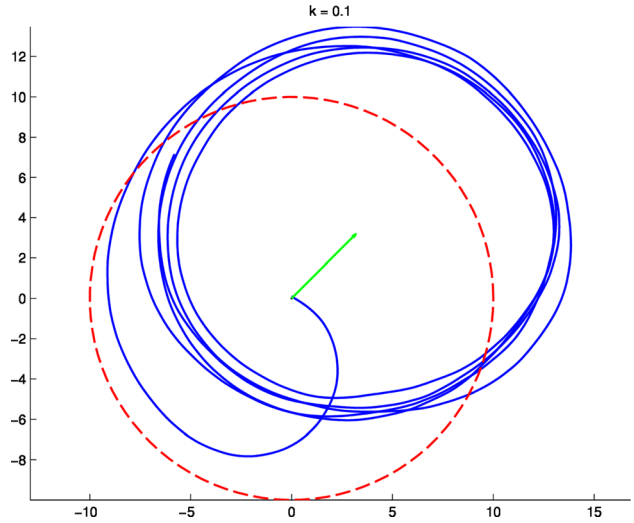

Fig. 12 Trajectory with measurement error and wind, $k = 0.1$

correspond to less radial error at the expense of smoothness and large control effort; though only to a point. If the maximum control adjustment $2kV$ is larger than π (here corresponding when $k = \pi/2$), then the UAV may turn directly around instantaneously. Besides being quite impractical, this causes the UAV to overcorrect and spin out of control.

6.2 Measurement Error With Constant Wind. Here, we examine the performance of the algorithm under the influence of measurement errors (as described in Sec. 6.1) and constant wind. One may formulate the "windy" system with constant wind bias of speed W_s and direction w_d as

$$d\begin{bmatrix} x \\ y \\ \psi \end{bmatrix} = \begin{bmatrix} V\cos\psi + W_s\cos w_d \\ V\sin\psi + W_s\sin w_d \\ u \end{bmatrix} dt + \begin{bmatrix} 0 \\ 0 \\ -k\sigma \end{bmatrix} d\xi \qquad (22)$$

We simulate trajectories under such a wind model, using the same control policy u as in Eq. (8). We take the windspeed $W_s = V/4 = 0.25$ and the wind direction $w_d = \pi/4$. Figures 12 and 13 depict the windy trajectories analogous to the windy case. We note that with the minimal gain size the trajectory forms a circular orbit, but is shifted off-target in the direction of the wind. When the gain is turned up the UAV adjusts more dynamically and is able to adhere to the desired radius much better.

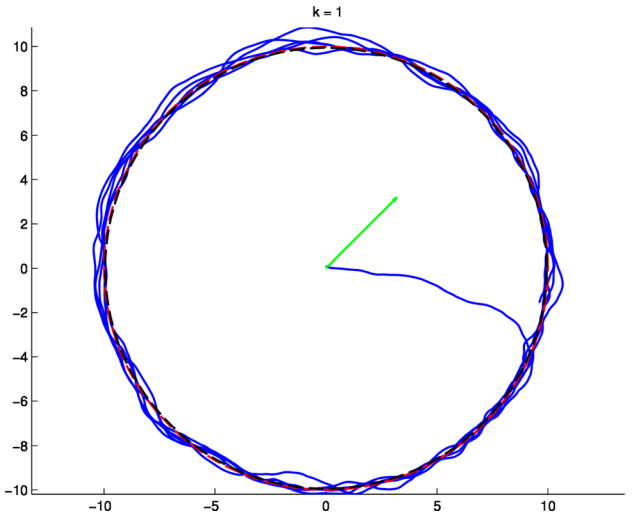

Fig. 13 Trajectory with measurement error and wind, $k = 1$

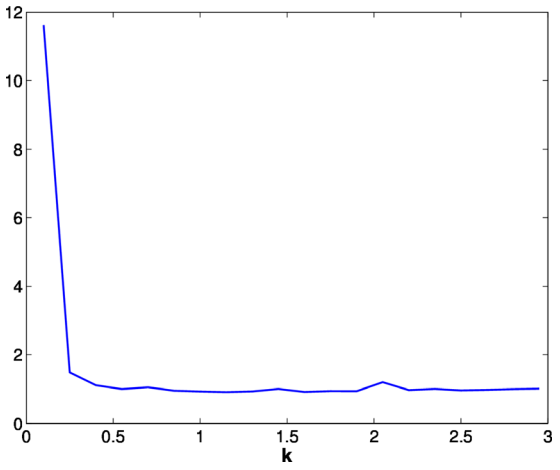

Fig. 14 Average value of error $(r - r_d)^2$ with wind

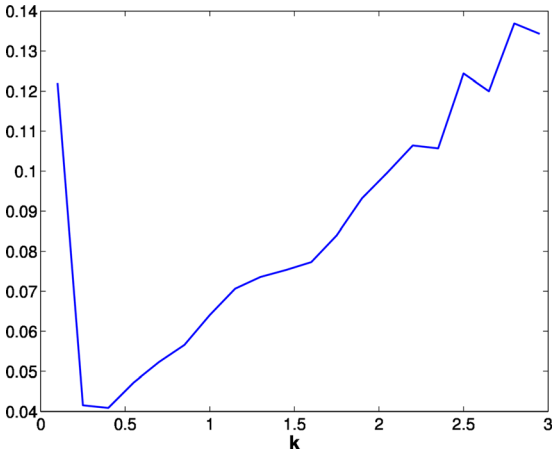

Fig. 15 Average value of $\dot{r}^2$ with wind

Figures 14 and 15 show the mean-square error of $(r - r_d)$ and $\dot{r}$ under the influence of wind and measurement errors. We mention that we have also simulated trajectories with randomly varying wind (with wind speed and direction modeled by Ornstein-Uhlenbeck processes) with very similar results. With small gain one observes bias in the average trajectory, and with large enough

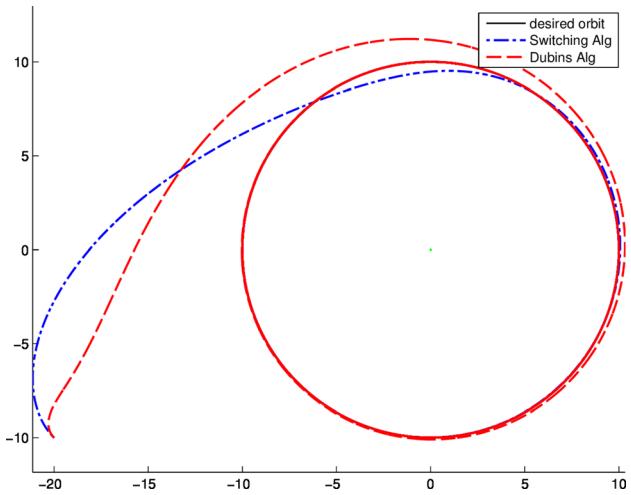

Fig. 16 Deterministic trajectory with exact r, estimated $\dot{r}$

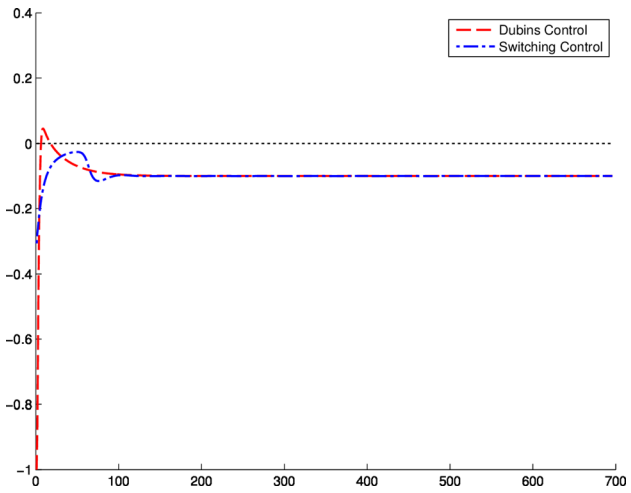

Fig. 17 Deterministic control applied with exact r, estimated $\dot{r}$

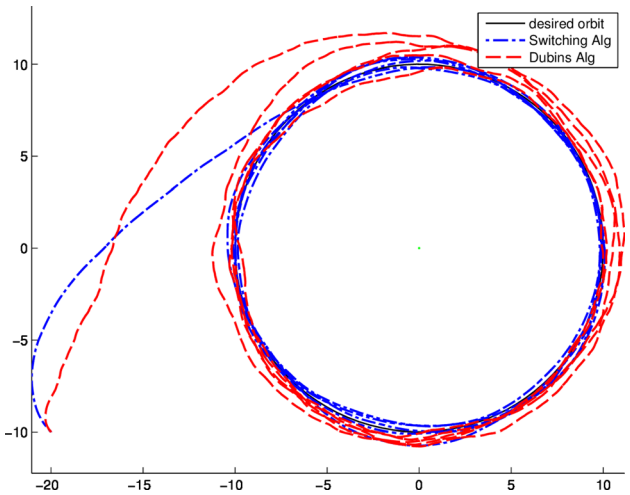

Fig. 18 Trajectory with exact r, noisy $\dot{r}$ ($\sigma_{rr} = 0.5$), time step $h = 0.1$ s

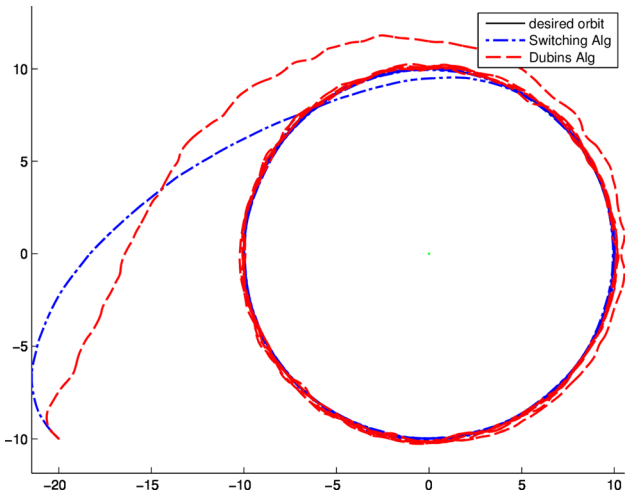

Fig. 19 Trajectory with noisy r ($\sigma_r = 0.1$), estimated $\dot{r}$, time step $h = 0.5$ s

gain the control is able to adapt to the varying wind. We thus omit the figures for brevity.

6.3 Comparison With Dubins Controller. Here we compare the performance of the switching controller and the "Dubins" controller proposed in Ref. [11]. The Dubins controller in Ref. [11] has the following form of $u = \text{sat}(u_c)$ with:

$$u_c = \frac{1}{\sqrt{V^2 - \dot{r}^2}} \left(\frac{c_1(r-d)}{c_2} + \frac{V^2 - \dot{r}^2}{r} + c_3 \dot{r} \right) \tag{23}$$

where $\text{sat}(\cdot)$ is the saturation function modeling the physical turning constraints of the UAV and c_i, $i = 1,2,3$ are positive constants. Here, we take the saturation bound to be $w_{\max} = 1$ for a reasonable maximum control applied at each time step. We take the initial point for both controllers to be $(x(0), y(0), \psi(0)) = (-20, -10, 3\pi/4)$ and take velocity $V = 1$. Using this initial information, we tune the parameters for the Dubins control to be $c_1 = 0.08$, $c_2 = 1$, and $c_3 = 1.1$. For the switching controller, we take gain size $k = 0.25$. In addition, we apply the same saturation function to the output of the switching controller for better comparison with the Dubins.

We illustrate the comparable deterministic performance in Figs. 16 and 17. Similar to Ref. [11] we use exact range measurements $\hat{r} = r$ and estimated measurements of $\dot{r}$ by using difference quotients from values of r: $\hat{\dot{r}}_t = (1/h)(r_t - r_{t-h})$. Here, the time step increment is taken to be $h = 0.5$ s. One sees that both controllers quickly converge to the desired orbit with very little control effort. We note that throughout the Dubins controller is graphed in red and the switching controller is graphed in blue.

We now investigate the comparative performance with noise under two different noise models. The first model, "exact r, noisy $\dot{r}$" is similar to Sec. 6.1. In this case, range measurements are exact $\hat{r} = r$ and range-rate measurements are corrupted by i.i.d. noise $\hat{\dot{r}}_t \sim \mathcal{N}(\dot{r}_t, \sigma_{rr}^2)$ with $\sigma_{rr} = 0.5$. We note that this is a fairly large variance relative to the velocity $V = 1$. Controls are then updated frequently by increments of $h = 0.1$ s to take advantage of averaging (since the noise is i.i.d.). Figures 18–23 depict the comparative performance. We note while both controllers applied similar control in the deterministic case (Fig. 17), with this (large) noise model the switching control has significantly less control effort.

The second model, "noisy r, estimated $\dot{r}$," assumes the range measurements are noisy such that $\hat{r}_t \sim \mathcal{N}(r_t, \sigma_r^2)$ with $\sigma_r = 0.1$ (small noise). The range-rate measurements $\dot{r}$ are then estimated from measurements of r as before: $\hat{\dot{r}}_t = (1/h)(\hat{r}_t - \hat{r}_{t-h})$. Thus we see that $\hat{\dot{r}}_t \sim \mathcal{N}\big((1/h)(r_t - r_{t-h}), (1/h^2)2\sigma_r^2\big)$. The choice of time

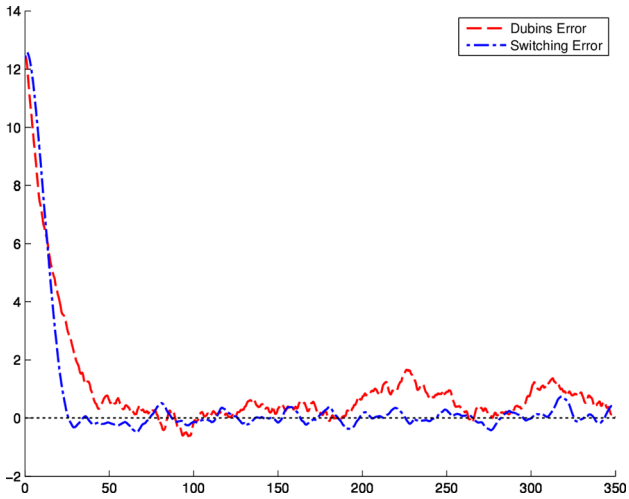

Fig. 20 Error with exact r, noisy $\dot{r}$ ($\sigma_{\dot{r}} = 0.5$), time step $h = 0.1$ s

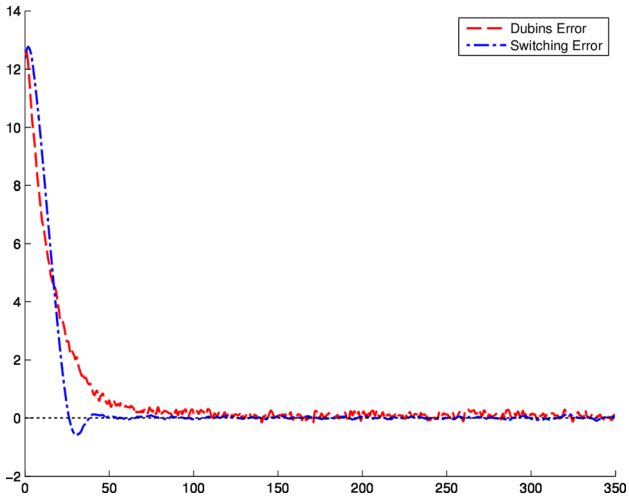

Fig. 21 Error with noisy r ($\sigma_r = 0.1$), estimated $\dot{r}$, time step $h = 0.5$ s

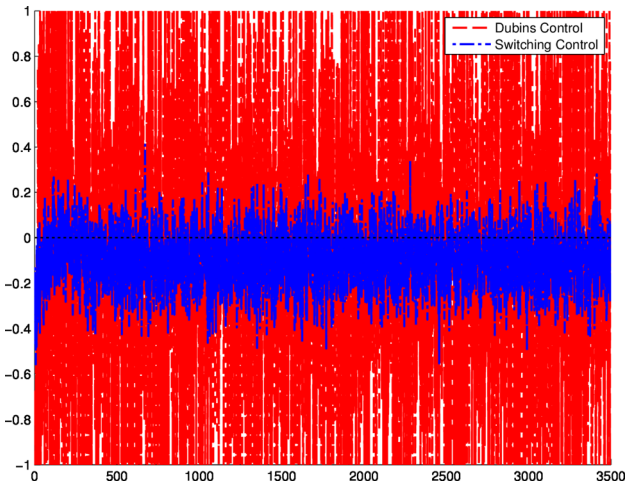

Fig. 22 Control with exact r, noisy $\dot{r}$ ($\sigma_{\dot{r}} = 0.5$), time step $h = 0.1$ s

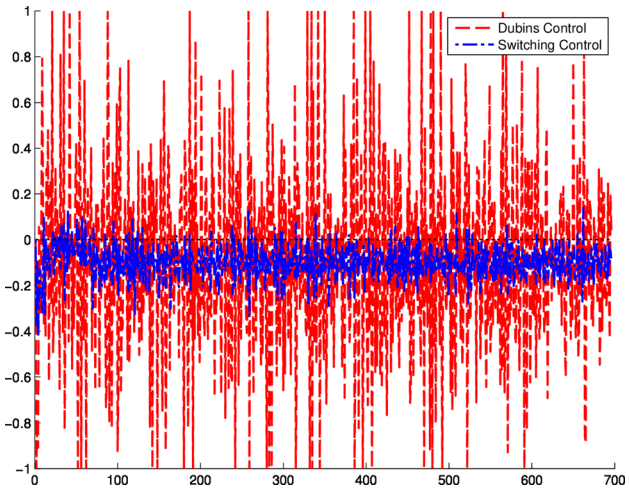

Fig. 23 Control with noisy r ($\sigma_r = 0.1$), estimated $\dot{r}$, time step $h = 0.5$ s

step h leads to a bias-variance trade-off problem one often sees in estimation problems. For the simulation we take a relaxed time step of $h = 0.5$ s to keep the variance reasonable. Again, we observe similar performance between the two algorithms, but a smaller control effort for the switching controller.

7 Conclusion and Future Work

This paper has developed and analyzed a robust control policy for a UAV to circumnavigate a stationary target using noise-corrupted range and range-rate measurements, without any of the location information that would be unavailable in a GPS-denied environment. Under the assumption of additive measurement errors, we established a recurrence result that bounds the time until the UAV reaches a neighborhood of the desired orbit. Simulation studies were used to obtain statistical measures of performance and to compare with other control algorithms for the circumnavigation mission.

Our future effort aims to establish generalized notion of stability of the trajectory in the set in which it is recurrent to. Because the noise is persistent and does not decay near the equilibrium point, classic notions of stochastic stability are not applicable. One direction that may be considered is pth-moment set-wise stability in the sense of Ref. [14].

Acknowledgment

This work has been supported in part by AFOSR LRIR: 12RB07COR. The work of Yongcan Cao was supported by a National Research Council Research Associateship Award at AFRL.

Appendix

Claim: Control input u defined in Eq. (8) is Lipschitz with linear growth.

Proof. From Eq. (8), we see that $u(r,\theta) = kV\cos\theta - (kV/r)\sqrt{r^2 - r_s^2}\mathbb{I}_{\{r>r_s\}} + (kV/r_s)\sqrt{r_s^2 - r^2}\mathbb{I}_{\{r<r_s\}}$. The first term is a trig function of θ and thus globally Lipschitz with linear growth. For the second term, since kV is constant, let's consider the function $f(r) = (1/r)\sqrt{r^2 - s^2}$. Because $f(r) = O_r(1)$, it certainly has linear growth. Also, the derivative of $f(r)$ with respect to r is given by $f'(r) = (s^2/(r^2\sqrt{r^2 - s^2}))$, which is uniformly bounded on domains bounded away from $\{r = r_s\}$. As a consequence, $f(r)$ is Lipschitz on said domains. Similarly, the third term has linear growth and is Lipschitz away from $\{r = r_s\}$. Finally, the sum $-(\sqrt{r^2 - r_s^2}/r) + (\sqrt{r_s^2 - r^2}/r_s)$ is continuous at the

point $r = r_s$, and so is Lipschitz continuous in a sufficiently small neighborhood of $r = r_s$. Putting the above together indicates that $u(r,\theta)$ has linear growth and is Lipschitz. □

References

[1] Kearns, A., Shepard, D., Bhatti, J., and Humphreys, T., 2014, "Unmanned Aircraft Capture and Control via GPS Spoofing," J. Field Rob., **31**(4), pp. 617–636.

[2] Sahinoglu, Z., and Genzici, S., 2006, "Ranging in the IEEE 802.15.4a Standard," IEEE Wireless and Microwave Technology Conference, WAMICON 06, IEEE Annual, Clearwater Beach, FL, Dec. 4–5.

[3] Tang, Z., and Ozguner, U., 2005, "Motion Planning for Multitarget Surveillance With Mobile Sensor Agents," IEEE Trans. Rob., **21**(5), pp. 898–908.

[4] Summers, T., Akella, M., and Mears, M., 2009, "Coordinated Standoff Tracking of Moving Targets: Control Laws and Information Architectures," J. Guid., Control, Dyn., **32**(1), pp. 56–69.

[5] Deghat, M., Shames, I., Anderson, B., and Yu, C., 2014, "Localization and Circumnavigation of a Slowly Moving Target Using Bearing Measurements," IEEE Trans. Autom. Control (accepted).

[6] Shames, I., Dasgupta, S., Fidan, B., and Anderson, B., 2012, "Circumnavigation Using Distance Measurements Under Slow Drift," IEEE Trans. Autom. Control, **57**(4), pp. 889–903.

[7] Matveev, A., Teimoori, H., and Savkin, A., 2009, "The Problem of Target Following Based on Range-Only Measurements for Car-Like Robots," IEEE Conference on Decision and Control, held jointly with the 28th Chinese Control Conference, CDC/CCC 2009, Shanghai, China, Dec. 15–18, pp. 8537–8542.

[8] Cao, Y., Muse, J., Casbeer, D., and Kingston, D., 2013, "Circumnavigation of an Unknown Target Using UAVs With Range and Range-Rate Measurements," IEEE 52nd Annual Conference on Decision and Control, Firenze, Dec. 10–13, pp. 3617–3622.

[9] Hashemi, A., Cao, Y., Casbeer, D., and Yin, G., 2014, "UAV Circumnavigation of an Unknown Target Without Location Information Using Noisy Range-Based Measurements," Proceedings of the IEEE American Control Conference, Portland, OR, June 2014, pp. 4587–4592.

[10] Cao, Y., 2014, "UAV Circumnavigation of an Unknown Target Using Range Measurements and Estimated Range Rate," Proceedings of the IEEE American Control Conference, Portland, OR, June 2014, pp. 4581–4586.

[11] Øksendal, B., 2003, *Stochastic Differential Equations: An Introduction With Applications*, Springer-Verlag, Berling, Heidelberg.

[12] Khasminskii, R., 2011, *Stochastic Stability of Differential Equations*, Springer-Verlag, Berling, Heidelberg.

[13] Multinovic, D., Casbeer, D., Cao, Y., and Kingston, D., 2014, "Coordinate Frame Free Dubins Vehicle Circumnavigation," Proceedings of the IEEE American Control Conference, Portland, OR, June 2014, pp. 891–896.

[14] Mateos-Núñez, D., and Cortés, J., 2013, "Stability of Stochastic Differential Equations With Additive Persistent Noise," American Control Conference, Washington, DC, June 17–19, pp. 5427–5432.